Cement and Concrete Research 42 (2012) 769–777

Contents lists available at SciVerse ScienceDirect

Cement and Concrete Research

journal homepage: http://ees.elsevier.com/CEMCON/default.asp

Effects of accelerated carbonation on the microstructure of Portland cement pastes containing reactive MgO

Liwu Mo [a,b], Daman K. Panesar [a,*]

[a] Department of Civil Engineering, University of Toronto, ON, Toronto, Canada M5S 1A4
[b] College of Materials Science and Engineering, Nanjing University of Technology, Nanjing, 210009, China

ARTICLE INFO

Article history:
Received 15 September 2011
Accepted 23 February 2012

Keywords:
Microstructure (B)
Carbonation (C)
Acceleration (A)
MgO (D)
Characterization (B)

ABSTRACT

Reactive MgO is produced at a lower kiln temperature compared to ordinary Portland cement (OPC) and gains its physical properties mainly as a result of carbonation processes. Use of reactive MgO as cement replacement has recently gained attention in context with precast concrete products subjected to carbonation curing. This study investigates pastes containing 0–40% reactive MgO and the effect of accelerated carbonation curing on the: formation of new carbonate phases, microstructural development, and microhardness. Outcomes from this study revealed that the primary Ca and Mg-bearing carbonates formed are calcite, aragonite, magnesium calcite, and nesquehonite. The combined effect of carbonation and reactive MgO resulted in: a reduction in pore size and total pore volume, increase in apparent density, and greater microhardness compared to OPC paste. The chemical processes, and physical properties revealed that the dense inter-connected network structure consisting of Ca and Mg carbonates is a significant factor that influences the microhardness.

1. Introduction

The cement manufacturing process is a significant contributor to CO_2 emissions, and in fact, represents approximately 5% anthropogenic global CO_2 emissions [1]. Owing to increasing concerns regarding climate change mitigation, the cement industry is challenged with reducing its CO_2 emissions. Consequently, approaches are being developed to: improve the energy efficiency of burning; use alternative fuels and/or raw materials; promote grinding efficiency; and explore the role of cement systems in carbon capture and storage technologies [2]. Research and development of alternative cementitious binders with lower energy demands and CO_2 emissions is warranted and is of interest to the construction industry, cement producers, engineers and material scientists [2,3].

Utilization of reactive magnesia (MgO) as general use Portland cement replacement is a relatively new type of cementitious material which is typically produced by calcining magnesite ($MgCO_3$) at markedly lower temperatures, (i.e. <750 °C [4]), than the sintering temperature (up to 1450 °C) of Portland cement clinker. The reactive MgO gains its physical properties primarily as a result of carbonation processes. During carbonation, CO_2 is absorbed and chemically combined into carbonate phases which partially contributes to reducing CO_2 levels. The use of reactive MgO as cement replacement is of relevance and interest in context with prefabricated concrete products that can be cured in an environment with elevated CO_2 concentrations prior to use.

Carbonation of cement containing reactive MgO as cement replacement has been shown to improve the mechanical properties such as the stiffness, toughness, elastic modulus, and compressive strength of cementitious materials [5,6]. The improved mechanical properties are considered to be attributed to the densification of materials caused by the formation of magnesium carbonates, i.e. nesquehonite ($MgCO_3.3H_2O$) [5,6], dypingite ($Mg_5(CO_3)_4(OH)_2.5H_2O$) and artinite ($Mg_2(OH)_2CO_3.3H_2O$) [6]. However, no quantitative evidence of densification has been provided and the implications of the carbonated microstructure on the performance of reactive MgO systems remains unclear. The precipitation of magnesium carbonates in an aqueous MgO-CO_2-H_2O system has been investigated [7,8]. Studies have indicated that the reaction path and products of MgO-CO_2-H_2O system in solution are kinetically controlled and influenced by many factors such as temperature, CO_2 pressure, and ionic strength [7,8]. Nevertheless, the carbonation of reactive MgO, in the presence of Portland cement systems and its influence on the microstructure of cement paste is not well understood.

In contrast to carbonation in aqueous systems, the carbonation rate of bulk cement materials is influenced by the relative humidity of the environment which affects the penetration of CO_2. For conventional concrete, it has been well reported that the occurrence of carbonation reactions are most prominent between 40% and 80% relative humidity. Many researchers have used a range of 65% to 70% relative humidity in accelerated laboratory carbonation chambers for tests on conventional cement [9–11]. However, the carbonation of cement blended with reactive MgO requires a sufficient supply of water for the formation of

* Corresponding author at: Department of Civil Engineering, University of Toronto, 35 St. George St., Toronto, Ont., Canada M5S 1A4. Tel.: +1 416 946 5712; fax: +1 416 978 6813.
E-mail address: d.panesar@utoronto.ca (D.K. Panesar).

0008-8846/$ – see front matter © 2012 Elsevier Ltd. All rights reserved.
doi:10.1016/j.cemconres.2012.02.017

magnesium carbonates, and so accelerated carbonation chambers for cement-based materials containing reactive MgO are more effective at a higher relative humidity (i.e. 98%) [5,6]. The concentration and pressure of CO_2 also influence the carbonation rate of cement materials. In general, increasing CO_2 concentration and pressure facilitates diffusion processes and the dissolution of CO_2. Accelerated laboratory carbonation studies have typically used 2%–20% concentration of CO_2 when examining conventional Portland cement systems [9–12]. Similar to conventional Portland cement, CO_2 concentration has a strong influence on the carbonation processes of cement containing reactive MgO [5,13]. In natural conditions with atmospheric CO_2 concentration (0.03%–0.04%), the carbonation of reactive MgO was shown to be relatively slow [13]. However, researchers have shown that increasing the CO_2 concentration accelerated the rate of carbonation of reactive MgO-based cement [5,13]. Vandeperre et al. [5] found that cement pastes containing reactive MgO exposed to 20% concentration of CO_2 and 98% of relative humidity carbonated faster than specimens exposed to 5% concentration of CO_2 and a 65% relative humidity. De Silva et al. [14] exposed specimens mixed with various contents of portlandite ($Ca(OH)_2$) and brucite ($Mg(OH)_2$) to an accelerated carbonation chamber with 1 atm and 20 atm CO_2, respectively. The study revealed that increasing CO_2 pressure increased the acidity of pore solution and more Mg^{2+} was available for carbonation reactions.

Since carbonation of Portland cement materials has been shown to contribute to the formation of a less porous microstructure [15] and improved compressive strength [16,17], up to 100% CO_2 curing conditions have been employed for some precast concrete applications [18–21]. Shi and Wu [22] revealed that in comparison to conventional steam curing, CO_2 curing demands less energy and could yield greater environmental benefits due to CO_2 consumption through carbonation reactions. Literature reports that an improvement in the compressive strength of masonry blocks containing reactive MgO was observed when exposed to accelerated carbonation curing consisting of 20% CO_2 concentration [5,13].

Exposure of reactive MgO based cement products to elevated CO_2 concentrations and a high relative humidity can have beneficial effects on the rate of strength gain and microstructural development. This study examines the behaviour of cement paste containing up to 40% reactive MgO as cement replacement when exposed to an accelerated carbonation environment (99.9% concentration of CO_2, 98% relative humidity) for up to 56 d. The formation of new phases and their implications on the physical microstructure and microhardness are examined. This knowledge is necessary to further evolve low CO_2 binders containing reactive MgO and the development of potential applications.

2. Experimental

2.1. Materials, sample preparation and curing

General use Portland cement used in this study was supplied by Holcim Canada. The reactive MgO was supplied by Liyang Special Materials Company, China, which was produced by calcining $MgCO_3$ at approximately 800 °C. Table 1 presents the chemical composition of the cement and the reactive MgO. The reactive MgO mainly consists of magnesia, and a small amount of undecomposed $MgCO_3$ also exists. The reactive MgO powders have a particle size less than 80 μm, and a specific surface area of 54.6 m^2/g measured by BET N_2 adsorption.

Table 1
Chemical compositions of general use Portland cement and reactive MgO (weight %).

	MgO	CaO	SiO_2	Al_2O_3	Fe_2O_3	Na_2O	K_2O	SO_3	LOI
Portland cement	2.34	60.94	19.24	5.43	2.36	0.22	1.11	4.11	3.06
Reactive magnesia	89.67	1.65	0.36	0.23	0.34	0.23	0.06	–	7.15

LOI: loss on ignition.

Four cement paste mix designs with a water-to-binder ratio (w/b) of 0.5 were examined in this study. The four mix designs are designated as M-0, M-10, M-20, and M-40 which represent cement pastes incorporating 0%, 10%, 20%, and 40% of reactive MgO as cement replacement, respectively. For each mix design, two 20×20×300 mm paste prisms were prepared. At the completion of casting, the prisms were cured in an environment with 23±2 °C, and 90% relative humidity for 24± 2 h, and then demoulded.

One set of prisms was cured in a non-carbonation environment consisting of natural CO_2 concentration of approximately 0.04%, a relative humidity of 98%, and a temperature of 23±2 °C until tested. The set of specimens stored in the non-carbonation environment will be representative of the non-carbonated specimens. The second set of prisms, referred to as the carbonated samples, were exposed to the accelerated carbonation environment with relative humidity of 98%, CO_2 concentration of 99.9%, and a temperature of 23±2 °C for 7 d, 28 d, and 56 d. Prior to placing the samples in the accelerated carbonation chamber they were placed under vacuum using a LEYBOLD TRIVAC D8A pump for 24 h in a desiccator with silica gel in order to remove excess moisture from the cement pastes. This was conducted to facilitate the carbonation process [23]. The vacuum dried samples were placed in a sealed chamber under vacuum to remove the air from the chamber. The compressed CO_2 from a gas cylinder was first injected into a large (1000 L) plastic buffer bag. The CO_2 pressure in the buffer bag was equal to the atmospheric pressure. When the buffer bag was full of 99.9% CO_2 concentration, it was then connected to the chamber. The CO_2 then entered the chamber until the CO_2 pressure in the chamber was equal to the atmospheric pressure. Consequently, as carbonation processes proceeded, CO_2 was supplied continuously from the buffer bag. The buffer bag was refilled with CO_2 from the compressed CO_2 cylinder before the CO_2 was completely consumed. To ensure sufficient availability of water necessary for the formation of magnesium carbonates [5,6], a target of 98% relative humidity in the chambers was achieved with saturated K_2SO_4 solution [24].

2.2. Test procedures

For each mix design, 12–13 mm thick slices were sawn from the paste prisms after 7 d, 28 d and 56 d of curing. The slices were vacuum dried for 72 h by using the same drying method described in Section 2.1. The paste slices were used for the microhardness test, X-ray diffraction (XRD) analysis and differential thermal analysis (DTA)/ thermogravimetric (TG) analysis, pore structure investigation, scanning electron microscopy (SEM), backscattered electron (BSE) imaging and energy dispersive X-ray (EDX) analysis. However, prior to testing the paste specimens cured in the accelerated carbonation chamber, the carbonation front was examined by spraying 1% phenolphthalein pH-indicator to the fresh-split surfaces of the pastes.

2.2.1. Microhardness test

The microhardness was tested with a type 5100 Buehler Microhardness tester. The surfaces of the sawn slices were polished with silicon carbide abrasive particle coated papers starting from 240 grit paper and continuing with 400, 600, 2400, and 4000 grit paper. Upon completion of polishing, the samples were tested with a Vickers diamond pyramid indenter. A load of 0.981 N was applied with a dwell time of 10 s. A minimum of nine indentations were made on each sample. In general, it is reported that Vickers microhardness of cement materials has a positive correlation with compressive strength [25–27].

2.2.2. Chemical analysis – XRD and DTA/TGA

For chemical analysis, the paste samples were ground into a powder with a maximum particle size of 80 μm. The XRD analysis was performed using an Analytical X-Ray Powder Diffractometer with Cu Kα

radiation ($\lambda = 1.5418$ Å), 2θ range of 5°–80°, and a step size of 0.02° to identify the presence of crystalline phases.

The DTA/TG analysis was performed using a NETZSCH STA 409 instrument. Once powder samples were placed in the equipment, they were heated at a uniform rate of 10 °C/min from 25 °C to 1050 °C with a nitrogen gas flow of 50 ml/min. The results were used to estimate the CO_2 uptake for the various curing durations.

2.2.3. Pore structure and image analysis – MIP, SEM, and BSE

Mercury Intrusion Porosimetry (MIP) was conducted using a Quantachrome Autoscan 60 mercury intrusion porosimeter. The samples tested were approximately 2 g, with a maximum dimension of 2–3 mm. Quantification of the total porosity, pore size distribution, and the apparent densities was determined from MIP testing.

A JEOL JSM6610-Lv SEM coupled with an Oxford Silicon Drift Detector EDX spectroscopy was used for image and chemical analysis of the paste samples. The morphology of the carbonate phases was examined using SEM on gold coated specimens. The BSE images were also prepared using the JEOL JSM6610-Lv SEM equipment. For BSE image analysis, the dried slice samples were impregnated with epoxy resin. After the epoxy hardened, the samples were polished with 240, 400, 600, 2400, and 4000 grit abrasive paper and then polished using two oil lubricates, the first containing 9 μm diamonds followed by 3 μm diamonds. The polished samples were carbon coated before analysis.

3. Results and discussion

3.1. Carbonation front

After 7 d, 28 d, and 56 d of carbonation curing, fresh split surfaces of M-0, M-10, M-20, and M-40 were sprayed with 1% phenolphthalein solution. None of the samples showed an obvious colour change, indicating that the CO_2 penetrated through the specimen's entire transverse-section as early as 7 d of curing in the accelerated carbonation chamber.

3.2. Microhardness

Table 2 shows the influence of age on the Vickers microhardness of carbonated and non-carbonated cement pastes containing up to 40% reactive MgO. The data presented is the mean of nine measurements and the corresponding coefficients of variation for the microhardness ranges from 6% to 16%.

The microhardness of non-carbonated cement pastes were measured at 28 d and 56 d. As shown in Table 2, the microhardness values of all the non-carbonated cement pastes increased with age. With the increasing percentage of MgO as cement replacement, the microhardness decreased slightly at 28 d.

Cement paste exposed to the accelerated carbonation environment experienced a relatively rapid rate of microhardness gain with age. Table 2 shows that after only 7 d of exposure to CO_2, the mean microhardness values of carbonated pastes containing reactive MgO were greater than all of the non-carbonated pastes after 56 d except for M-40. After 7 d of carbonation, approximately 90%, 86%, 86%, and 54% of the 56 d mean microhardness was achieved for the M-0, M-10, M-20, and M-40 mixtures, respectively. Although the microhardness of the M-40 paste at 7 d carbonation was relatively lower than mixtures M-0, M-10, M-20, it was observed that the mean microhardness of M-40 at 56 d of carbonation was 700 MPa, being close to 728 MPa of M-20.

Table 2
Microhardness of carbonated and non-carbonated cement pastes containing 0–40% reactive MgO. (mean ± standard deviation, MPa).

	Exposure time (d)	M-0	M-10	M-20	M-40
Carb.	7	451 ± 53	563 ± 52	629 ± 77	379 ± 28
	28	441 ± 63	609 ± 47	670 ± 81	571 ± 91
	56	502 ± 63	653 ± 70	728 ± 85	700 ± 52
Non-carb.	28	235 ± 26	212 ± 25	203 ± 19	150 ± 14
	56	404 ± 56	412 ± 62	379 ± 22	422 ± 47

3.3. X-ray diffraction analysis

Figs. 1a and 1b illustrate the XRD patterns of cement pastes containing 0 to 40% reactive MgO after 7 d and 56 d of carbonation, respectively. After 7 d of carbonation, calcite was the main calcium carbonate formed in the M-0 paste, as well as a relatively smaller amount of aragonite as shown in Fig. 1a. In addition to calcite, it was expected that for carbonated samples containing 10–40% reactive MgO, magnesium calcite would form by incorporating Mg^{2+} in $CaCO_3$ during the precipitation process. However, calcite and magnesium calcite generally show similar 2θ values which make it difficult to distinguish between them using XRD patterns [14]. However, this was examined further and will be discussed in Section 3.6. In carbonated pastes containing reactive MgO, there were some weak peaks of $MgCO_3$ which may be due to the undecomposed $MgCO_3$ present in the reactive MgO (raw material). This is further supported by studies which report that the formation of $MgCO_3$ is kinetically inhibited in 'low' temperature environments including room temperature [7,8]. Small diffraction peaks of magnesia (MgO) and brucite ($Mg(OH)_2$) were observed for M-20 paste, indicating that some MgO and $Mg(OH)_2$ were uncarbonated. For the M-40 paste, clear diffraction peaks of brucite ($Mg(OH)_2$), portlandite ($Ca(OH)_2$) and MgO were observed indicating that some of these phases remained uncarbonated.

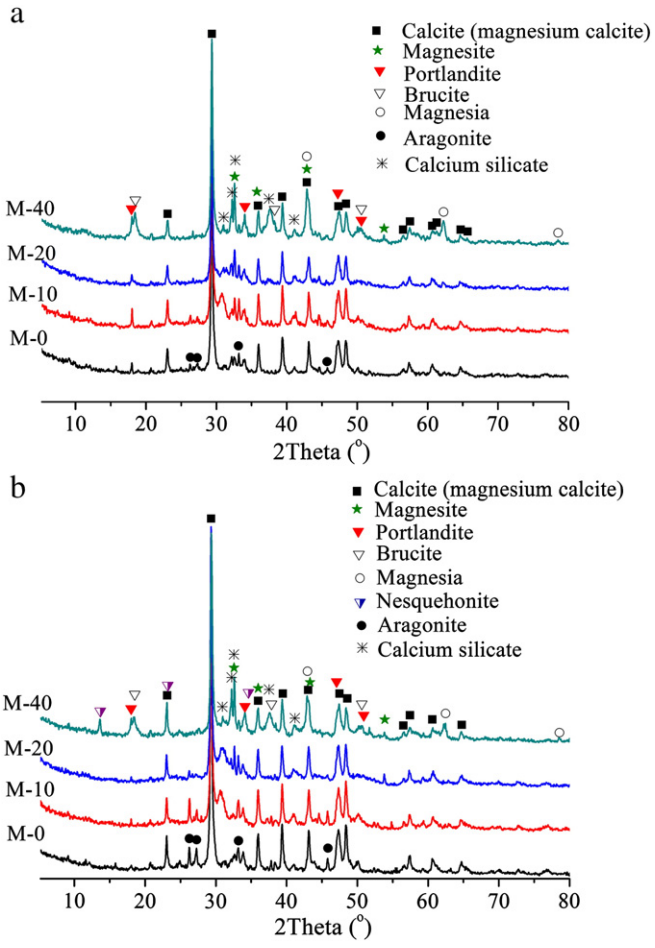

Fig. 1. XRD patterns of cement pastes containing 0–40% reactive MgO after a) 7 d of carbonation curing and b) 56 d of carbonation curing.

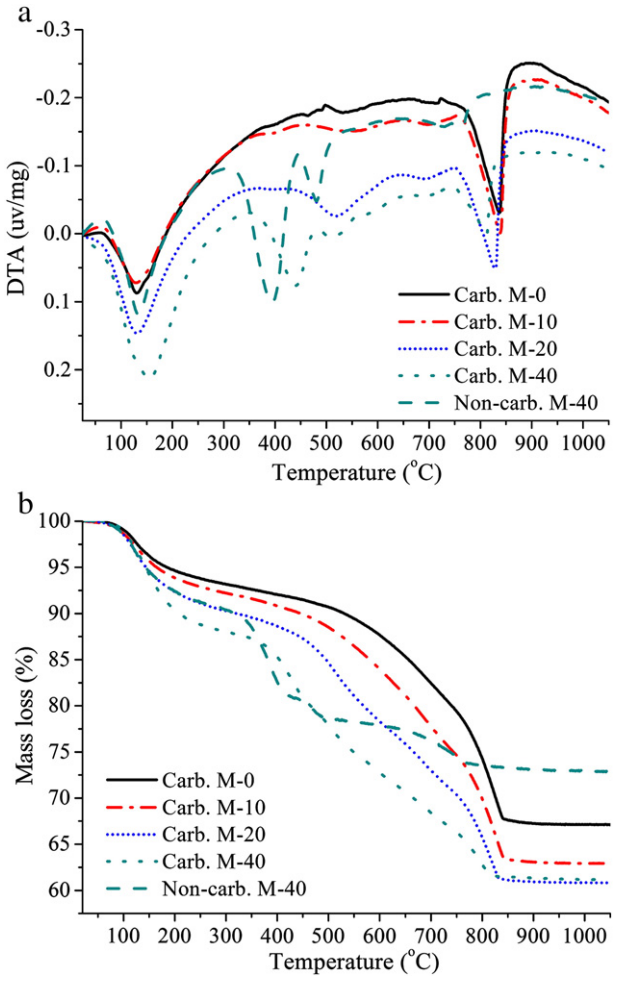

Fig. 2. Carbonated and non-carbonated cement pastes after 56 d of curing a) DTA curves, and b) TG curves.

Comparing Fig. 1a with Fig. 1b indicates that the carbonates formed in M-0, M-10, and M-20 after 56 d of carbonation curing were generally the same as those formed after 7 d of carbonation curing but with three noteworthy exceptions. Firstly, for paste mixture M-40, nesquehonite ($MgCO_3.3H_2O$) was formed as evidenced by its diffraction peaks in Fig. 1b. Secondly, by increasing the addition of reactive MgO, the diffraction intensity of aragonite decreased. And thirdly, after 7 d of carbonation curing, $Mg(OH)_2$ and MgO were identified in the M-10 and M-20 samples, but the phases were no longer present after 56 d of carbonation curing indicating that they had eventually carbonated. However, for the M-40 carbonated mixture, the diffraction peaks of $Mg(OH)_2$, $Ca(OH)_2$, and MgO presented at 7 d, indicative of uncarbonated phases, were still present after 56 d.

3.4. Differential thermal and thermogravimetric analysis

Fig. 2a and b, respectively, show the DTA and TG curves of carbonated and non-carbonated paste specimens after 56 d of curing. For the non-carbonated M-40 samples, two clear endothermic peaks at 390 °C and 480 °C are related to the decomposition of $Mg(OH)_2$ and $Ca(OH)_2$, respectively. In addition, a weak endothermic peak appears at 765 °C which may relate to the decomposition of limestone in GU cement. (Less than 5% limestone is incorporated in the general use Portland cement.) In contrast, Fig. 2a reveals only one obvious endothermic peak at 837 °C for the carbonated M-0 paste which is related to the decarbonation of $CaCO_3$. Although for the carbonated M-0, Fig. 2b clearly shows a weight loss between 500 °C and 750 °C but no corresponding endothermic peaks are evident in Fig. 2a. This may be associated with the decarbonation of amorphous $CaCO_3$. Thiery et al. [28] proposed that three decomposition modes of $CaCO_3$ at 550 °C–680 °C, 680 °C–780 °C, and 780 °C–990 °C exist, which correspond respectively to, amorphous calcium carbonate, vaterite and aragonite, and well-crystallized calcite.

For carbonated cement pastes containing reactive MgO, the decarbonation peak temperature of $CaCO_3$ decreased slightly compared to M-0, which may be associated with the formation of magnesium calcite. Moreover, it seems that subtle overlapped endothermic peaks appeared between 500 °C and 750 °C, particularly in M-20 and M-40 samples, which is accompanied by a clear mass loss as shown in Fig. 2b. This may be related to the decarbonation of magnesium calcite, $MgCO_3.3H_2O$, and $MgCO_3$. The latter mainly decarbonated between 500 °C and 650 °C [29], while the former, $MgCO_3.3H_2O$, first dehydrates at 440 °C to form $MgCO_3$ and then decarbonates at 550 °C [30]. Fig. 2a shows that for carbonated M-40 paste, a clear endothermic region ranging from 350 °C to 500 °C occurs which is attributed to overlapping dehydration peaks of $Ca(OH)_2$, $Mg(OH)_2$ and $MgCO_3.3H_2O$. Owing to the overlapping peaks, it was difficult to distinguish the weight loss corresponding to the decomposition of each phase. However, it was expected that most of the weight loss between 500 °C and 850 °C is related to the decarbonation of calcium and magnesium carbonates.

To further examine the weight loss in the 500 °C–850 °C region, estimates of the total CO_2 uptake of cement during the carbonation process were calculated. Table 3 presents the estimates which were based on the weight loss corresponding to 500 °C–850 °C shown in Fig. 2b. It should be noted that, the estimation does not account for the limestone incorporated in the general use cement, and the undecomposed magnesite in reactive MgO. As shown in Table 3, most of the CO_2 was absorbed within the first 7 d of carbonation curing. The CO_2 uptake remained almost constant from 28 d to 56 d for the M-0 and M-10 specimens, however, the M-20 and M-40 pastes did exhibit a slight increase of CO_2 uptake which is expected to be related to the continuous formation of Mg-bearing carbonates. At 56 d of carbonation curing, the CO_2 uptake expressed as the percentage of the weight of carbonated samples is 23.0%, 25.2%, 23.6%, and 16.2% for M-0, M-10, M-20, and M-40 samples, respectively. The paste consisting of 40% MgO experienced the lowest CO_2 uptake which was also supported by the XRD analysis which revealed that some MgO, $Mg(OH)_2$, and $Ca(OH)_2$ remained uncarbonated even after 56 d of carbonation.

3.5. Pore structure and apparent density

Pore size distributions of the M-0 and M-20 paste specimens are shown in Fig. 3 for curing durations up to 56 d. The pore size in all samples decreased with the increasing carbonation ages regardless of the presence of reactive MgO. Fewer changes to the pore structure were observed between 28 d and 56 d compared to between 7 d and 28 d. This is supported by the results in Table 3, which shows that more CO_2 was absorbed during the carbonation period from 7 d to 28 d compared to that from 28 d to 56 d.

Table 3
Total CO_2 uptake in carbonated cement pastes (by weight of carbonated samples, weight %).

	M-0			M-10			M-20			M-40		
Exposure time (d)	7	28	56	7	28	56	7	28	56	7	28	56
Total CO_2 uptake	21.0	23.1	23.0	22.8	25.0	25.2	21.8	22.9	23.6	14.6	15.7	16.2

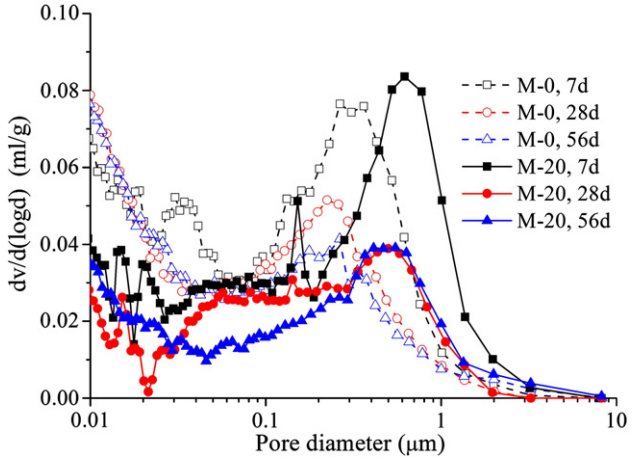

Fig. 3. Pore size evolution of M-0 and M-20 after different days of carbonation.

Fig. 4 shows the pore size distributions of cement pastes containing up to 40% reactive MgO after 56 d of curing in both, the non-carbonation and accelerated carbonation chambers. The results show that the pore volumes were markedly lower for the carbonated samples compared to the non-carbonated samples at all levels of reactive MgO as cement replacement. Closer examination revealed that irrespective of the presence of reactive MgO, the carbonated pastes had a relatively lower volume of fine pores, 0.02–0.1 μm. The M-40 pastes experienced a relatively greater volume of coarser pores, 0.4–1 μm, for both the carbonated and non-carbonated samples.

Table 4 presents the total pore volume of carbonated and non-carbonated cement pastes with age. With increasing addition of reactive MgO, the total pore volume of non-carbonated pastes at 56 d increased from 0.163 ml/g of M-0 to 0.180 ml/g of M-40. This may be associated with lower amount of calcium silicate hydrate (C-S-H) present with increasing cement replacement percentages of reactive MgO. The total pore volumes of the carbonated samples were much lower in comparison to the non-carbonated pastes. Table 4 shows that the total pore volumes of all carbonated samples were equal to or less than 0.135 ml/g after only 7 d of carbonation and continued to decrease, albeit at a slower rate. In contrast to the non-carbonated cement pastes, the total pore volume of carbonated cement pastes decreased with increasing percentages of reactive MgO. After 56 d of carbonation, the total pore volumes of M-0, M-10, M-20, and M-40 paste were 0.108 ml/g, 0.096 ml/g, 0.077 ml/g, and 0.073 ml/g, respectively.

Accompanying the reduction in pore size and total pore volume, the apparent densities of cement pastes also increased with increasing

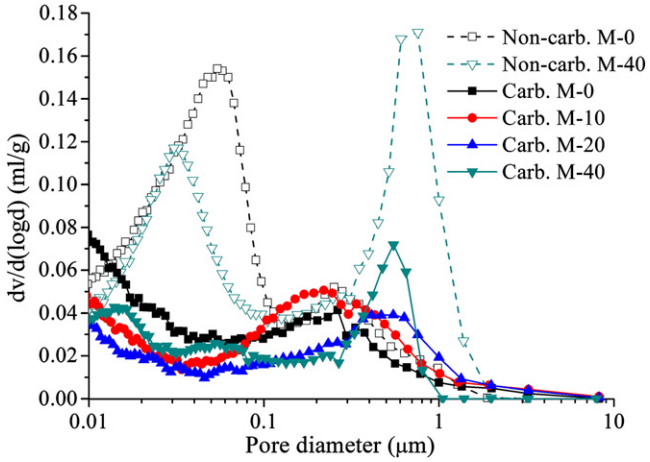

Fig. 4. Pore size distributions of non-carbonated and carbonated cement pastes containing various contents of MgO after 56 d of exposure.

Table 4
Total pore volumes of carbonated and non-carbonated cement pastes containing various contents of reactive MgO. (ml/g).

	Exposure time (d)	M-0	M-10	M-20	M-40
Carb.	7	0.135	0.114	0.113	0.135
	28	0.116	0.096	0.079	0.085
	56	0.108	0.096	0.077	0.073
Non-carb	56	0.163	0.176	0.173	0.180

formation of carbonates. Table 5 reveals that after only 7 d of carbonation, the apparent densities of carbonated pastes containing 0 to 40% of reactive MgO were larger than that of non-carbonated pastes after 56 d curing. At 56 d, the apparent densities of carbonated M-0, M-10, M-20, and M-40 were 1.905 g/ml, 1.958 g/ml, 2.015 g/ml, and 1.900 g/ml respectively, being greater than that of non-carbonated samples which ranged from 1.580 g/ml to 1.648 g/ml. Based on a mineral database, the densities of $Ca(OH)_2$ and $CaCO_3$ are 2.23 g/ml and 2.71 g/ml, respectively [31] and so transformation of $Ca(OH)_2$ (per mole) into $CaCO_3$ can yield an 11.2% increase in solid volume. The densities of MgO, $Mg(OH)_2$, $MgCO_3$, and $MgCO_3.3H_2O$ are 3.78 g/ml, 2.39 g/ml, 3.00 g/ml, and 1.84 g/ml, respectively [31]. The transformation of MgO (per mole) to $Mg(OH)_2$, $MgCO_3$, and $MgCO_3.3H_2O$, could result in a solid volume increase of approximately 128.7%, 166.7%, and 604.8%, respectively. The apparent densities of carbonated cement pastes increase with the increasing percentage of reactive MgO except for M-40. This can be partially explained by the XRD results reported in Section 3.3 which revealed that the M-40 paste had some MgO, $Mg(OH)_2$, and $Ca(OH)_2$ which remained uncarbonated.

The influence of MgO on the correlation between porosity and microhardness of cement pastes is shown in Fig. 5. The microhardness increased with decreasing total pore volume, indicating that less porous pastes correspond to a relatively greater microhardness and vice versa.

3.6. Microstructural characterization

3.6.1. SEM morphology of carbonates

Fig. 6 shows the SEM image of cement paste M-0 at 56 d of carbonation. The figure illustrates the well-crystallized rhombohedral $CaCO_3$ formed in pores and around pore walls. The size of the relatively large $CaCO_3$ crystal was approximately 0.4 μm. Smaller $CaCO_3$ was formed away from pores as shown in the bottom left region of Fig. 6.

Fig. 7 shows the SEM image of carbonates formed in the M-40 paste after 56 d of carbonation curing. Carbonates with round faces and edges were formed in the pores and on the pore walls of the paste. The EDX elemental analysis of point 1 in Fig. 7, reveals the presence of both Mg and Ca in the round-faced carbonates, suggesting that the carbonates were magnesium calcite. This is supported by the results shown in Fig. 1b. These carbonates were observed to be approximately 0.8 μm which is larger than the $CaCO_3$ observed in the M-0 carbonated cement paste sample. Greater amounts of round magnesium calcite were observed in pastes with increasing percentages of reactive MgO. Magnesium calcite was formed due to the incorporation of Mg^{2+} into $CaCO_3$ during the precipitation process in the supersaturated solution [32].

Table 5
Apparent densities of carbonated and non-carbonated cement pastes containing various contents of reactive MgO. (g/ml).

	Exposure time (d)	M-0	M-10	M-20	M-40
Carb.	7	1.779	1.824	1.839	1.682
	28	1.864	1.905	1.965	1.873
	56	1.905	1.958	2.015	1.900
Non-carb	56	1.648	1.611	1.600	1.580

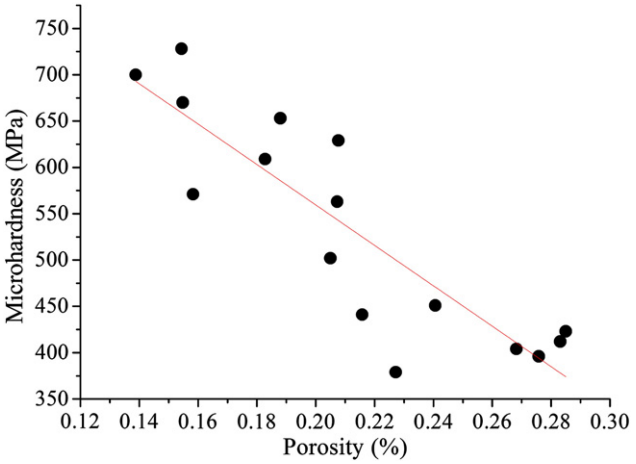

Fig. 5. Relationship between the porosity and microhardness.

Figs. 6 and 7 show the morphology of the calcite and magnesium calcite, respectively. Fig. 6 illustrates rhombohedral $CaCO_3$ in M-0 paste, whereas with the incorporation of reactive MgO, the carbonates are round tightly agglomerated crystal aggregates (Fig. 7). The incorporation and the abundance of Mg^{2+} have been reported to affect the crystal morphology of $CaCO_3$ due to its influence on the crystal nucleation and growth process [33–36]. It is expected that the incorporation of Mg in $CaCO_3$ which promoted the aggregation of $CaCO_3$ crystals would be beneficial to the strength of paste.

3.6.2. BSE investigation on microstructure

Fig. 8 shows the BSE image of the M-0 cement paste after 56 d of carbonation. Rims consisting of agglomerated $CaCO_3$ were formed around the pores, and some large agglomerates of $CaCO_3$ also precipitated in the pores.

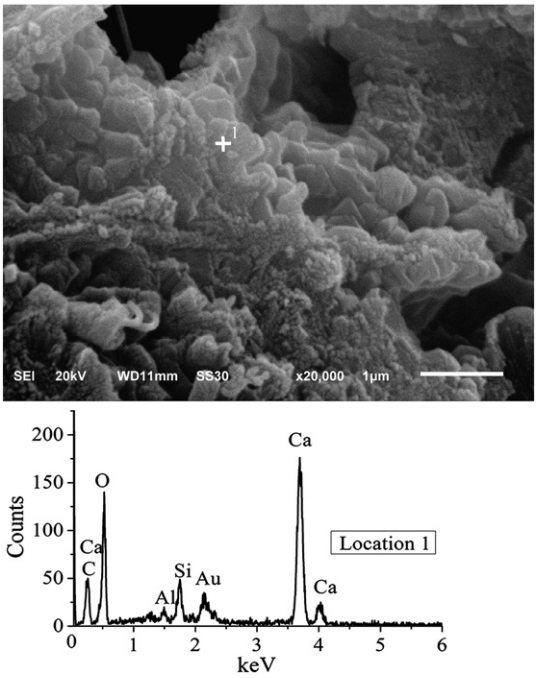

Fig. 6. SEM morphology image of calcite formed in M-0 after 56 d of carbonation.

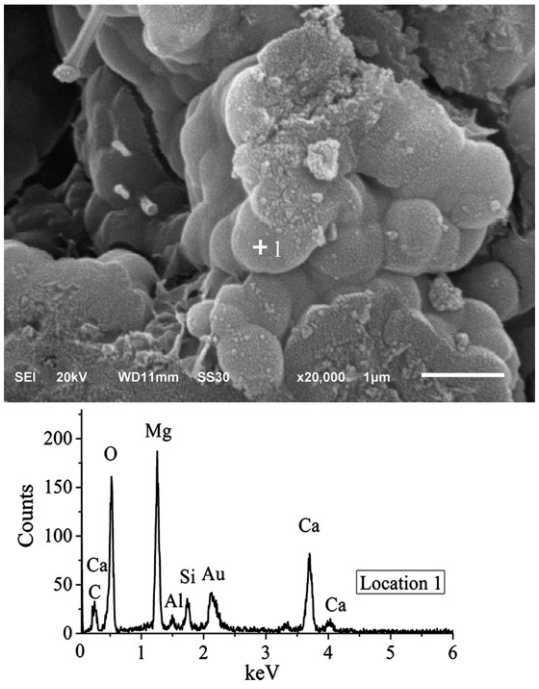

Fig. 7. SEM image of magnesium calcite formed around pore in M-40 after 56 d of carbonation.

Fig. 9 shows the BSE image of carbonated M-20 paste coupled with the elemental compositions analyzed by EDX. Similar to carbonated M-0 samples, carbonate rims were formed around the pores in the paste. However, the carbonation rims of the M-20 paste mainly consist of $CaCO_3$ and magnesium calcite due to the incorporation of Mg in $CaCO_3$. The EDX analysis results in Fig. 9 present the Mg/Ca ratios at locations 1, 2, 3, and 4 which ranges from 0.10 to 0.72. This indicates the content of Mg incorporated in calcite varied depending on the location. In Fig. 9, locations 1 and 2 correspond to the label "D: high magnesium calcite" and the reported Mg/Ca ratios at location 1 and 2 were also relatively high in comparison to locations 3 and 4. This analysis suggests that the high-magnesium carbonates were formed locally due to the diffusion of CO_3^{2-} and Ca^{2+} to the inner pores of reactive MgO and surrounded by the Ca-bearing carbonates (i.e. calcite, low-magnesium calcite).

Fig. 10a shows the BSE image of M-40 after 7 d of carbonation illustrating the $Mg(OH)_2$ surrounded by Ca-bearing carbonates and a band of Ca-bearing carbonates formed in brucite, due to the

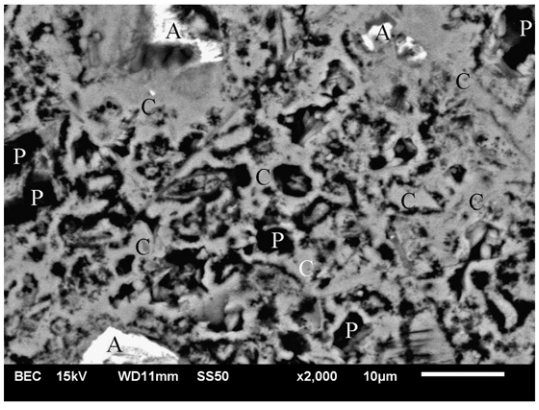

Fig. 8. BSE images of M-0 paste at 56 d of carbonation (A: anhydrous clinker, C: calcite, P: pore).

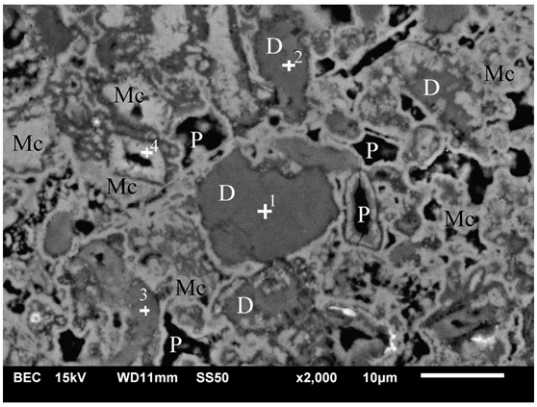

Elemental composition analysis on locations 1, 2, 3 and 4 (weight%)

	C	Mg	Si	S	Ca	O	Mg/Ca ratio (by weight)
1	13.0	13.4	0.8	1.0	18.5	53.3	0.72
2	14.1	11.5	1.3	1.0	17.2	55.0	0.67
3	11.6	9.2	5.3	1.2	19.2	52.9	0.48
4	13.2	2.9	0.8	1.1	30.3	51.7	0.10

Fig. 9. BSE image of M-20 paste at 56 d of carbonation coupled with chemical compositions at locations 1, 2, 3, and 4. (D: high-magnesium calcite, Mc: magnesium calcite, P: pore).

diffusion of Ca^{2+} into the reactive MgO particle and precipitation of magnesium carbonates. After 56 d of carbonation, as shown in Fig. 10b, nesquehonite ($MgCO_3.3H_2O$) was formed around the $Mg(OH)_2$ in the M-40 cement paste, which may be formed due to the carbonation of $Mg(OH)_2$. Wilson et al. [37] reported the similar plate texture of $MgCO_3.3H_2O$ as that illustrated in Fig. 10b.

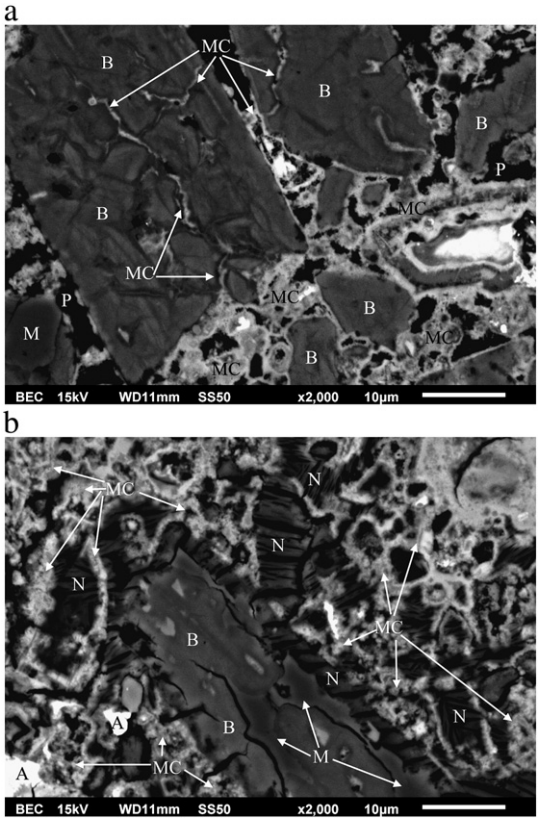

Fig. 10. BSE image of M-40 paste at a) 7 d of carbonation and b) 56 d of carbonation (A: anhydrous cement clinker, B: $Mg(OH)_2$, P: pore, M: $MgCO_3$, MC: magnesium calcite, N: $MgCO_3.3H_2O$).

Furthermore, the $MgCO_3.3H_2O$ was surrounded by Ca-bearing carbonates (calcite and magnesium calcite), which indicated it was formed locally.

3.7. Discussion

3.7.1. Carbonation of Portland cement pastes containing reactive MgO

For general use Portland cement, the carbonation process involved primarily: (i) dissolution of $Ca(OH)_2$, (ii) CO_2 absorption and formation of carbonate ions in water, and (iii) chemical reaction and precipitation of $CaCO_3$ [15]. Ca^{2+} could also be provided by the decalcification of C-S-H gel, ettringite, and even unhydrated C_2S and C_3S [15,38]. A supersaturated solution of $CaCO_3$ was formed then $CaCO_3$ precipitated as described in Eq. (1).

$$Ca^{2+}(aq) + CO_3^{2+}(aq) \rightarrow CaCO_3(s) \quad (1)$$

$CaCO_3$ precipitated as well-crystallized large crystals in the pore solution and on the pore walls. In some cases the precipitated calcium carbonates from the pore solution could partially fill the pores while simultaneously forming a dense carbonate layer on the pore wall. This could eventually obstruct CO_2 ingress from the external environment whereby the carbonation process is controlled by diffusion. As carbonation processes proceed, CO_2 penetrated through the $CaCO_3$ layer and reacted with Ca^{2+} (from the decalcification of C–S–H, C_3S and C_2S) and was expected to contribute to the formation of relatively small and amorphous $CaCO_3$ [38].

For cement pastes containing reactive MgO as cement replacement, the Mg^{2+} ions were provided by MgO and its hydration product, $Mg(OH)_2$. The supersaturated pore solution containing both Ca^{2+} and Mg^{2+} enabled the formation of various Ca- and Mg-bearing carbonates with the latter dependant on the abundance of Mg, which could be generally described in Eq. (2).

$$Ca^{2+}(aq) + Mg^{2+}(aq) + {CO_3}^{2-}(aq) \rightarrow Ca_xMg_{1-x}CO_3(s) \quad (2)$$

The potential for carbonate phases to incorporate Mg during the precipitation process was associated with the saturation index of $MgCO_3$ in solution [32]. Increasing Mg^{2+} concentration in solution increased the Mg content in calcite crystals [33].

In comparison to $Mg(OH)_2$, $Ca(OH)_2$ has higher solubility, and thus more Ca^{2+} ions can be dissolved in the pore solution [39,14]. Similar to the carbonates formed in paste M-0, for the M-20 and M-40 pastes, Ca-bearing carbonates (i.e. calcite, magnesium calcite) precipitated in the pores, on the pore walls, and around the $Mg(OH)_2$ or MgO particles to form dense carbonate layers as shown in Figs. 9 and 10. This may consequently lead to obstructing the penetration of CO_2, and reducing the rate of carbonation reactions.

Owing to the low solubility of $Mg(OH)_2$, only a small amount of Mg^{2+} dissolved into the pore solution which limited the carbonation rate of MgO and the transport of Mg^{2+} into the cement paste. Moreover, the dense Ca-bearing carbonate layer formed around $Mg(OH)_2$ may also block and limit the diffusion of Mg^{2+} ions yielding a Mg^{2+} rich region around the surface of MgO or $Mg(OH)_2$. The CO_3^{2-} and Ca^{2+} ions diffused through the carbonate layer into the high Mg^{2+} concentration region and precipitated locally. In Mg^{2+} concentration rich environment, greater amounts of Mg^{2+} would be incorporated into $CaCO_3$ to form high-magnesium calcite, and even $MgCO_3.3H_2O$ [14,32]. The formation of $MgCO_3.3H_2O$ can be described as:

$$Mg^{2+}(aq) + {CO_3}^{2-}(aq) + H_2O(aq) \rightarrow MgCO_3.3H_2O(s) \quad (3)$$

In this study, $MgCO_3.3H_2O$ was formed only in paste samples containing 40% reactive MgO after 56 d of carbonation. Accordingly, carbonation products of reactive MgO may be a result of precipitation in pore solution or through localized reactions.

3.7.2. Microstructure evolution of the carbonated cement pastes

The primary hydration phases for non-carbonated cement pastes, are C-S-H, ettringite, $Ca(OH)_2$, and $Mg(OH)_2$ in M-10, M-20, and M-40 mixtures. Although the replacement of Portland cement by reactive MgO reduced the amount of C-S-H, which may negatively influence the densification of microstructure it has also been shown to yield a small increase in the total pore volume, as shown in Table 4 and supported by Vandeperre et al. [40]. On the other hand, the transformation of MgO into $Mg(OH)_2$ crystal results in a solid volume increase of 128.7% which may contribute towards densifying the microstructure, and to producing a stronger matrix than MgO powder. The counteracting processes, (i.e. pore volume increase and solid volume increase of MgO), could explain the 56 d microhardness data for the non-carbonated pastes shown in Table 2 which reveals that the percentage of MgO had a minimal influence on the microhardness particularly when the standard deviations were considered.

However, the carbonated cement pastes containing reactive MgO consisted mainly of calcium and magnesium carbonates, and some uncarbonated phases, i.e. C-S-H, $Ca(OH)_2$, and $Mg(OH)_2$ in M-40. Owing to the rapid formation of carbonates, the development of the microhardness of all the carbonated samples by 7 d was greater than that of the microhardness achieved by non-carbonated samples by 28 d (Table 2). This is closely associated with the development of the microstructure during the carbonation process. Figs. 8, 9, and 10 show the formation of an inter-connected network structure consisting of densely agglomerated Ca-bearing carbonates, while the carbonates of high-magnesium calcite and $MgCO_3.3H_2O$, along with the uncarbonated phases such as cement clinker, and $Mg(OH)_2$ acted as "micro-aggregates" inlaid in the network.

Three factors are likely to contribute to the microstructure evolution and its performance. Firstly, the strength of the network structure is related to the binding strength and the morphology of the carbonate crystals. De Silva et al. [41] reported that the morphology of carbonates, rather than the amount of carbonates, was the main factor controlling the performance of carbonate binders, and the network-like structure formed by inter-connected and well-developed crystals further enhanced its performance. Secondly, the decrease in total pore volume, and increase in apparent density due to the formation of carbonates may also have contributed to the performance of the microstructural network. Thirdly, the bulk "micro-aggregate" consisting of the high-magnesium calcite and $MgCO_3.3H_2O$ formed through localized carbonation is also expected to enhance the performance of binder matrix. By increasing the percentage of reactive MgO in cement paste, greater amounts of magnesium calcite were formed, and even $MgCO_3.3H_2O$ was identified in pastes with 40% MgO. These formations have been shown to yield a matrix with relatively lower pore volume in comparison to general use Portland cement pastes.

In this study, although the amount of CO_2 uptake of the M-40 paste was estimated to be the lowest after 56 d of carbonation as shown in Table 3, the mean microhardness value of M-40 was 700 MPa, being larger than 502 MPa of M-0, 653 MPa of M-10, and close to 728 MPa of M-20. This is attributed to the tightly agglomerated carbonates and dense microstructure due to the formation of magnesium calcite and $MgCO_3.3H_2O$.

4. Conclusions

Based on the aforementioned results and discussion, the primary concluding remarks are:

(i). The carbonation of all the paste specimens was effectively accelerated under the condition of 99.9% CO_2, 98% relative humidity and a temperature of 23 ± 2 °C. In Portland cement paste without reactive MgO, calcite and aragonite were the main calcium carbonates formed. For cement pastes containing reactive MgO, magnesium calcite was formed due to the incorporation of Mg^{2+} in the carbonate phase, and nesquehonite was formed only in pastes containing 40% reactive MgO.

(ii). Formation of both calcium and magnesium carbonates caused microstructure densification indicated by a reduction in total pore volume, increasing apparent density, and greater microhardness of cement pastes in comparison to non-carbonated specimens. Pastes containing 40% reactive MgO, resulted in a 32% reduction in total pore volume, and a 39% greater mean microhardness after 56 d of carbonation curing in comparison with 100% general use Portland cement pastes.

(iii). Ca-bearing carbonates (calcite, magnesium calcite) precipitated in the pores and formed dense carbonate layer around the pore wall. It is proposed that the carbonation of brucite and MgO contributed towards reducing the capillary pore volume and the inter-connectivity of the pores, barring penetration of CO_2 and in turn reducing the rate of carbonation. Magnesium carbonates (high-magnesium calcite and nesquehonite) were formed mainly through the localized reaction due to the limited diffusion of Mg^{2+}. The dense inter-connected microstructure, as a result of the formation of calcium and magnesium carbonates, may be an important factor that controls the performance of the carbonated cement pastes.

(iv). This study revealed valuable insight to the physico-chemical processes of using up to 40% reactive MgO in binder systems. Owing to the relatively lower calcining temperature of MgO coupled with its relatively higher CO_2 uptake through carbonation reactions, utilization of reactive MgO in cement has potential to have a lower environmental impact in comparison to general use Portland cement. However, further examination of the influence of reactive MgO on the properties (i.e. compressive strength, durability) of cement paste, mortar and concrete are needed in order to assess potential applications, and long term performance.

Acknowledgements

The authors are grateful to Ms. O. Perebatova, Prof. K. Peterson, and Prof. R.D. Hooton from the Civil Engineering Department, Dr. Daniel Grozea and Mr. Bill Tang from the Materials Science and Engineering Department, and Dr. George Kretschmann from the Geology Department in University of Toronto, Canada for their input and/or assistance with the experiments. Prof. Deng Min and Mr. Lu Anqun from Nanjing University of Technology, China are acknowledged for providing materials. Financial support from the China Scholarship Council/The University of Toronto Joint Scholarship program and the National Science and Engineering Research Council of Canada (NSERC) is greatly appreciated.

References

[1] Cement Technology Roadmap, Carbon emissions reductions up to 2050. International Energy Agency and World Business Council for Sustainable Development, 2009, p. 36, date accessed Sept. 13, 2011, http://www.wbcsd.org/DocRoot/mka1EKor6mqLVb9w903o/WBCSD-IEA_CementRoadmap.pdf.
[2] M. Schneider, M. Romer, M. Tschudin, H. Bolio, Sustainable cement production – present and future, Cem. Concr. Res. 41 (2011) 642–650.
[3] E.M. Gartner, D.E. Macphee, A physico-chemical basis for novel cementitious binders, Cem. Concr. Res. 41 (2011) 736–749.
[4] T. Tececo Pty Ltd. Australia, US Patent 7347896, (2008).
[5] L.J. Vandeperre, A. Al-Tabbaa, Accelerated carbonation of reactive MgO cements, Adv. Cem. Res. 19 (2007) 1–13.
[6] M. Liska, A. Al-Tabbaa, Ultra-green construction: reactive magnesia masonry products, Proceedings of the institution of civil engineers, Waste and resource management, 162, 2009, pp. 1–12, issue WR0.
[7] Y. Xiong, A.S. Lord, Experimental investigations of the reaction path in the MgO–CO_2–H_2O system in solutions with various ionic strengths, and their applications to nuclear waste isolation, Appl. Geochem. 23 (2008) 1634–1659.
[8] M. Hächen, V. Prigiobbe, R. Baciocchi, M. Mazzotti, Precipitation in the Mg-carbonate system—effects of temperature andCO_2 pressure, Chem. Eng. Sci. 63 (2008) 1012–1028.
[9] C.-F. Chang, J.-W. Chen, The experimental investigation of concrete carbonation depth, Cem. Concr. Res. 36 (2006) 1760–1767.

[10] K. Sisomphon, F. Lutz, Carbonation rates of concretes containing high volume of pozzolanic materials, Cem. Concr. Res. 37 (2007) 1647–1653.
[11] P. Sulapha, S.F. Wong, T.H. Wee, S. Swaddiwudhipong, Carbonation of concrete containing mineral admixtures, J. Mater. Civ. Eng. 15 (2003) 134–143.
[12] L. De Ceukelaire, D. Van Nieuwenburg, Accelerated carbonation of a blast-furnace cement concrete, Cem. Concr. Res. 23 (1993) 442–452.
[13] M. Liska, L.J. Vandeperre, A. Al-Tabbaa, Influence of carbonation on the properties of reactive magnesia cement-based pressed masonry units, Adv. Cem. Res. 20 (2008) 53–64.
[14] P. De Silva, L. Bucea, V. Sirivivatnanon, Chemical, microstructural and strength development of calcium and magnesium carbonate binders, Cem. Concr. Res. 39 (2009) 460–465.
[15] C.A. García-González, C. Andrade, M.C. Alonso, J. Fraile, A. López-Periago, Concepción Domingo, Modification of composition and microstructure of Portland cement pastes as a result of natural and supercritical carbonation procedures, Ind. Eng. Chem. Res. 45 (2006) 4985–4992.
[16] J.M. Chi, C.C. Ran Huang, C. Yang, Effects of carbonation on chemical properties and durability of concrete using accelerated testing method, J. Mar. Sci. Technol. 10 (2002) 14–20.
[17] S. Monkman, Y. Shao, Carbonation curing of slag-cement concrete for binding CO_2 and improving performance, J. Mater. Civ. Eng. 22 (2010) 296–304.
[18] S. Monkman, Y. Shao, Integration of carbon sequestration into curing process of precast concrete, Can. J. Civ. Eng. 37 (2010) 302–310.
[19] S. Monkman, Y. Shao, Assessing the carbonation behavior of cementitious materials, Can. J. Civ. Eng. 18 (2006) 768–776.
[20] C. Shi, Y. Wu, Studies on some factors affecting CO_2 curing of light weight concrete products, Resour. Conserv. Recycl. 52 (2008) 1087–1092.
[21] C. Shi, Q. Zou, Use of CO_2 as an accelerated curing agent for concrete blocks, Key Eng. Mater. 400–402 (2009) 81–87.
[22] C. Shi, Y. Wu, CO_2 curing of concrete blocks, Concr. Int. (February 2009) 39–43.
[23] M.A. Venhuis, E.J. Reardon, Vacuum method for carbonation of cementitious wasteforms, Environ. Sci. Technol. 35 (2001) 4120–4125.
[24] J.F. Young, Humidity control in the laboratory using salt solutions – a review, J. Appl. Chem. 17 (1967) 241–245.
[25] J.J. Beaudoin, R.F. Feldman, A study of mechanical properties of autoclaved calcium silicate systems, Cem. Concr. Res. 5 (1975) 103–118.
[26] R.F. Feldman, H. Chengyi, Properties of Portland cement-silica fume pastes, II. Mechanical properties, Cem. Concr. Res. 15 (1981) 943–952.
[27] S. Igarashi, A. Bentur, S. Mindess, Microhardness testing of cementitious materials, Adv. Cem. Based Mater. 4 (1996) 48–57.
[28] M. Thiery, G. Villain, P. Dangla, G. Platret, Investigation of the carbonation front shape on cementitious materials: effects of the chemical kinetics, Cem. Concr. Res. 37 (2007) 1047–1058.
[29] M. Samtani, D. Dollimore, K.S. Alexander, Comparison of dolomite decomposition kinetics with related carbonates and the effect of procedural variables on its kinetic parameters, Thermochim. Acta 392–393 (2002) 135–145.
[30] J. Lanas, J.I. Alvarez, Dolomitic lime: thermal decomposition of nesquehonite, Thermochim. Acta 421 (2004) 123–132.
[31] Mineralogy Database, http://webmineral.com (accessed September 15, 2011).
[32] O.S. Pokrovsky, Precipitation of calcium and magnesium carbonates from homogeneous supersaturated solutions, J. Cryst. Growth 186 (1998) 233–239.
[33] F.C. Meldrum, S.T. Hyde, Morphological influence of magnesium and organic additives on the precipitation of calcite, J. Cryst. Growth 231 (2001) 544–558.
[34] E. Lostea, R.M. Wilson, R. Seshadric, F.C. Meldrum, The role of magnesium in stabilising amorphous calcium carbonate and controlling calcite morphologies, J. Cryst. Growth 254 (2003) 206–218.
[35] J.O. Titiloye, S.C. Parker, S. Mann, Atomistic simulation of calcite surfaces and the influence of growth additives on their morphology, J. Cryst. Growth 131 (1993) 533–545.
[36] L. Fernandez-Dias, A. Putnis, M. Prieto, C.V. Putnis, The role of magnesium in the crystallisation of calcite and aragonite in a porous medium, J. Sediment. Res. 66 (3) (1996) 482–491.
[37] S.A. Wilson, G.M. Dipple, I.M. Power, J.M. Thom, R.G. Anderson, M. Raudsepp, J.E. Gabites, G. Southam, Carbon dioxide fixation within mine wastes of ultramafic-hosted ore deposits: examples from the Clinton Creek and Cassiar Chrysotile deposits, Canada, Econ. Geol. 104 (2009) 95–112.
[38] P.H.R. Borges, J.O. Costa, N.B. Milestone, C.J. Lynsdale, Roger E. Streatfield, Carbonation of CH and C–S–H in composite cement pastes containing high amounts of BFS, Cem. Concr. Res. 40 (2010) 284–292.
[39] A.J.W. Harrison, The case for and ramification of blending reactive magnesia with Portland cement, Presented at the 28th Conference on Our World in Concrete Structures, Singapore, August, 2003.
[40] L.J. Vandeperre, M. Liska, A. Al-Tabbaa, Microstructures of reactive magnesia cement blends, Cem. Concr. Compos. 30 (2008) 706–714.
[41] P. De Silva, L. Bucea, D.R. Moorehead, V. Sirivivatnanon, Carbonates binders: reaction kinetics, strength and microstructure, Cem. Concr. Compos. 28 (2006) 613–620.